Available online at www.sciencedirect.com
ScienceDirect
Chinese Journal of Aeronautics 22(2009) 551-557
Chinese Journal of Aeronautics
www.elsevier.com/locate/cja

Microscopic Phase-field Simulation of Effects of Re-ageing Temperature on Precipitation of Ni-Al-Cr Alloys

Zhang Jixiang[a,b,*], Chen Zheng[a], Lai Qingbo[a], Zhao Yan[a], Wang Yongxin[a]

[a]*School of Materials Science and Engineering, State Key Laboratory of Solidification Processing, Northwestern Polytechnical University, Xi'an 710072, China*

[b]*School of Materials Engineering, Yancheng Insititute of Technology, Yancheng 224051, China*

Received 4 September 2008; accepted 4 January 2009

Abstract

This article, by means of the ternary microscopic phase-field model, investigates the effects of re-ageing temperature on the precipitation of $Ni_{75}Al_{10}Cr_{15}$ alloy with the help of atomic pictures, order parameters, particle density, averaged radii, and volume fractions. During pre-ageing at 873 K, DO_{22} phases first appear through spinodal decomposition mechanism, and then $L1_2$ phases begin to form on the DO_{22} phase-boundaries through non-classical nucleation mechanism. In either of them, ordering process is obviously faster than atom clustering. At the late stage of re-ageing at 923 K, the elastic strain energy seems to exert stronger effects on microstructure, and DO_{22} and $L1_2$ phases exhibit directional alignment along ⟨100⟩ direction to a certain extent. When the temperature increases to 1 023 K, the influence of elastic strain energy begins to weaken, and the precipitated phases become randomly distributed in the matrix. The volume fraction of DO_{22} phase decreases to zero, whereas that of $L1_2$ phase first increases and then decreases with the temperature rising from 923 K to 1 123 K. On the whole, the effects of elastic strain energy make the coarsening behavior of both phases deviate from the time-law predictions by LSW diffusion-controlled growth theory.

Keywords: Ni-Al-Cr alloy; microscopic phase-field; re-ageing; nucleation; order parameter

1. Introduction

Most properties of metallic materials depend upon their internal microstructures. For precipitation-strengthened alloys, controlling the precipitate morphology by reasonable age hardening is one of most important measures to develop new alloys. As one of the key materials used in advanced aero-engines and industrial gas turbines, Ni-Al-Cr alloys have drawn considerable attention from both scientists and engineers in recent years[1]. The mechanical properties of this kind of Ni-based superalloys strongly depend on the distribution and size of the Ni_3X-type precipitate particles. Many domestic and foreign researchers have widely investigated the precipitation of Ni-Al-Cr alloys. However, they have laid main focus on the late stage of precipitation[2-5]. Limited by experimental conditions, lots of important information cannot be gathered, and, moreover, instantaneous microstructural changes in the early stage of precipitation are in no position to be discovered with experimental instruments.

Microscopic phase-field model is a deterministic method, in which atomic occupation probability is regarded as a field variable. It has an obvious advantage to acquire information about microstructural evolution and quantitative results such as concentration changes in highly non-linear and non-equilibrium kinetic system, so much so that it has found wide application in simulating the precipitation process in Al-Li[6], Ni-Al[7], and Ni-Al-V alloys[8-9] for it obviates the need for presupposing the phase structure or nucleation mechanism of new phases and uses the interatomic interactions within the system as the only input variables.

This article investigates the effects of re-ageing temperature on the precipitation of $Ni_{75}Al_{10}Cr_{15}$ alloy during two-step ageing with the help of microscopic phase-field method. It is hoped to be of use in improving the production technology of this kind of alloys.

2. Theoretical Methods

Microscopic diffusion equation developed by A. G. Khachaturyan[10] is actually the microscopic version of Cahn-Hilliard equation. In this model, the atomic con-

*Corresponding author. Tel.: +86-29-88474095.
E-mail address: zhangjixiangdoctor@yahoo.com.cn
Foundation items: National Natural Science Foundation of China (50671084); China Postdoctoral Science Foundation Funded Project (20070420218)

doi: 10.1016/S1000-9361(08)60140-5

figuration and the morphology of a ternary alloy are described by a single-site occupation probability function, $P_a(\boldsymbol{r}, t)$, $P_b(\boldsymbol{r}, t)$, and $P_c(\boldsymbol{r}, t)$, which represent the probabilities of finding an a, b, or c atom at a given lattice site $\boldsymbol{r}$ at given time t, respectively. Since in a ternary system, $P_a(\boldsymbol{r}, t) + P_b(\boldsymbol{r}, t) + P_c(\boldsymbol{r}, t) = 1.0$, only two equations are independent at each lattice. If $P_a(\boldsymbol{r}, t)$ and $P_b(\boldsymbol{r}, t)$ are assumed to be the independent variables, there will be two independent kinetic equations at each lattice site for species a and b, respectively. Then, the microscopic kinetic equation of a ternary system is

$$\left.\begin{aligned}\frac{\mathrm{d}P_a(\boldsymbol{r},t)}{\mathrm{d}t} &= \frac{1}{k_bT}\sum_{\boldsymbol{r}'}[L_{aa}(\boldsymbol{r}-\boldsymbol{r}')\frac{\partial F}{\partial P_a(\boldsymbol{r}',t)} + \\ &\quad L_{ab}(\boldsymbol{r}-\boldsymbol{r}')\frac{\partial F}{\partial P_b(\boldsymbol{r}',t)}] + \zeta(\boldsymbol{r},t) \\ \frac{\mathrm{d}P_b(\boldsymbol{r},t)}{\mathrm{d}t} &= \frac{1}{k_bT}\sum_{\boldsymbol{r}'}[L_{ba}(\boldsymbol{r}-\boldsymbol{r}')\frac{\partial F}{\partial P_a(\boldsymbol{r}',t)} + \\ &\quad L_{bb}(\boldsymbol{r}-\boldsymbol{r}')\frac{\partial F}{\partial P_b(\boldsymbol{r}',t)}] + \zeta(\boldsymbol{r},t)\end{aligned}\right\} \quad (1)$$

where $L_{\alpha\beta}(\boldsymbol{r}-\boldsymbol{r}')$is the exchange probability between a pair of atoms, α and β, at lattice sites $\boldsymbol{r}$ and $\boldsymbol{r}'$ per unit time, $\alpha, \beta = a, b$ or c; F is the total Helmholtz free energy of the system; T the temperature and k_b the Boltzmann constant; $\xi(\boldsymbol{r}, t)$ the thermal noise which is assumed to be Gaussian-distributed with the average value of zero.

By the mean field theory, the free energy F is approximately given by:

$$\begin{aligned}F = -\frac{1}{2}\sum_{\boldsymbol{r}}\sum_{\boldsymbol{r}'}[V_{ab}(\boldsymbol{r}-\boldsymbol{r}')P_a(\boldsymbol{r})P_b(\boldsymbol{r}') + \\ V_{bc}(\boldsymbol{r}-\boldsymbol{r}')P_b(\boldsymbol{r})P_c(\boldsymbol{r}') + V_{ac}(\boldsymbol{r}-\boldsymbol{r}')P_a(\boldsymbol{r})P_c(\boldsymbol{r}')] + \\ k_bT\sum_{\boldsymbol{r}}[P_a(\boldsymbol{r})\ln(P_a(\boldsymbol{r})) + P_b(\boldsymbol{r})\ln(P_b(\boldsymbol{r})) + \\ P_c(\boldsymbol{r})\ln(P_c(\boldsymbol{r}))]\end{aligned} \quad (2)$$

in which, as an effective interchange interaction energy between α and β ($\alpha, \beta = a, b$, or c), $V_{\alpha\beta}(\boldsymbol{r}-\boldsymbol{r}')$ includes chemical interaction $V_{\alpha\beta}(\boldsymbol{r}-\boldsymbol{r}')_{\mathrm{at}}$ and elastic interaction $V_{\alpha\beta}(\boldsymbol{r}-\boldsymbol{r}')_{\mathrm{el}}$[11], i.e.

$$V_{\alpha\beta}(\boldsymbol{r}-\boldsymbol{r}') = V_{\alpha\beta}(\boldsymbol{r}-\boldsymbol{r}')_{\mathrm{at}} + V_{\alpha\beta}(\boldsymbol{r}-\boldsymbol{r}')_{\mathrm{el}} \quad (3)$$

For chemical interaction $V_{\alpha\beta}(\boldsymbol{r}-\boldsymbol{r}')_{\mathrm{at}}$, it seems to be more precise in describing free energy to use atom interaction up to the fourth neighbor owing to the transition and possible arrangement of three kinds of atoms in ternary system.

$V_{\alpha\beta}^1$, $V_{\alpha\beta}^2$, $V_{\alpha\beta}^3$, $V_{\alpha\beta}^4$ represent the first, second, third and fourth nearest-neighbor interaction energy parameters respectively. In the reciprocal space, the following equation is given:

$$\begin{aligned}V_{\alpha\beta}(\boldsymbol{k})_{\mathrm{at}} = 4V_{\alpha\beta}^1[\cos(\pi h)\cos(\pi k) + \cos(\pi h)\cos(\pi l) + \\ \cos(\pi k)\cos(\pi l)] + 2V_{\alpha\beta}^2[\cos(2\pi h) + \cos(2\pi k) + \cos(2\pi l)] + \\ 8V_{\alpha\beta}^3[\cos(2\pi h)\cos(\pi k)\cos(\pi l) + \cos(\pi h)\cos(2\pi k)\cos(\pi l) + \\ \cos(\pi h)\cos(\pi k)\cos(2\pi l)] + 4V_{\alpha\beta}^4[\cos(2\pi h)\cos(2\pi k) + \\ \cos(2\pi h)\cos(2\pi l) + \cos(2\pi k)\cos(2\pi l)]\end{aligned} \quad (4)$$

where $\boldsymbol{k}$ is the corresponding lattice site after transformation in the reciprocal space; h, k, l are coordinates of the reciprocal lattice sites.

In Ref.[8] and Ref.[12], the following interaction parameters are assumed: for Ni/Al interactions (meV/atom), $V_{\mathrm{Ni/Al}}^1 = 112.30$, $V_{\mathrm{Ni/Al}}^2 = 6.00$, $V_{\mathrm{Ni/Al}}^3 = 16.58$, and $V_{\mathrm{Ni/Al}}^4 = -6.82$; for Ni/Cr interactions (meV/atom), $V_{\mathrm{Ni/Cr}}^1 = 84.80$, $V_{\mathrm{Ni/Cr}}^2 = -46.80$, $V_{\mathrm{Ni/Cr}}^3 = -10.40$, and $V_{\mathrm{Ni/Cr}}^4 = -33.20$; for Al/Cr interactions (meV/atom), $V_{\mathrm{Al/Cr}}^1 = 140.00$, $V_{\mathrm{Al/Cr}}^2 = -40.00$, $V_{\mathrm{Al/Cr}}^3 = -74.50$, and $V_{\mathrm{Al/Cr}}^4 = 0$.

After Fourier transformation and long wave approximation, the function $V(\boldsymbol{k})_{\mathrm{el}}$ in 2D model can be written into

$$V(\boldsymbol{k})_{\mathrm{el}} \approx B(\boldsymbol{e}) \approx B(e_x{}^2e_y{}^2 - 0.125) \quad (5)$$

$$B = -\frac{4(c_{11}+2c_{12})^2}{c_{11}(c_{11}+c_{12}+2c_{44})}\varepsilon_0{}^2\Delta \quad (6)$$

where e_x and e_y are components of the unit vector $\boldsymbol{e}$ along the x-axis and y-axis in the reciprocal space and B is a material constant, which characterizes the elastic properties and the crystal lattice mismatch. In Eq.(6), $\varepsilon_0 = \mathrm{d}a(c)/(a_0\mathrm{d}c)$ is the concentration coefficient of crystal lattice expansion caused by the atomic size difference; $a(c)$ and a_0 are the crystal lattice parameters of solute and solid solution separately; c is the molar fraction of solute atoms; $\Delta = c_{11}-c_{12}-2c_{44}$ the elastic constant and c_{11}, c_{12}, c_{44} are elastic constants of the system under study[13]. In this simulation, we have $B > 0$, which holds for alloys with negative elastic anisotropy.

The computation work can be greatly simplified by substituting Eqs.(3)-(6) into Eq.(2) and then Eq.(2) into Eq.(1), which yields a reciprocal space representation of the ternary kinetic equation, and then transforming it from a 3D non-linear partial differential equation into a 2D linear constant differential one. The equation is solved with Euler method and the atomic figures and order parameters at different time are obtained from the atom occupation probability.

3. Results and Discussion

In the simulation, let simulation time be the actual time and the time step $\Delta t = 0.000\,1$, use 256×256 lattices and impose the periodic boundary conditions in both directions. The color scheme is so designed that a mix of different proportions of colors, white (standing for Al), gray (for Cr) and black (for Ni), at lattice sites represents the ratios of the occupation probability by different atoms. For example, if the occupation probability of Al at a site is 1.0, then the site is colored white. The rest is reasoned out by analogy. The $L1_2$ phase (Ni_3Al) therefore looks white, since the dominant color at the Cr sites is white. Similarly, the DO_{22} phase

(Ni_3Cr) gray. All Ni sites in both phases look black, which, therefore, makes a background. In addition, the ordered phase can also be identified by its arrangement pattern of atoms on 2D projection plane[14]. This article simulates the precipitation process of $Ni_{75}Al_{10}Cr_{15}$ alloy during two-step ageing, in which lower pre-ageing temperatures are adopted to generate more nuclei, and then finely distributed particles are obtained by re-ageing at a higher temperature. The pre-ageing temperature is 873 K all the time while the re-ageing temperatures are chosen to be 923 K, 1 023 K, and 1 123 K respectively. The pre-ageing time is 10 000 time steps, and the re-ageing time is 1 000 000 time steps. The initial state of the alloy is disordered oversaturated solid solution. Nucleation is accompanied by certain thermal noise, which is removed after nucleation. The system is allowed to select kinetics paths freely. The effects of re-ageing temperature on the precipitation mechanism and microstructure are pried with the help of acquired atom appearances and order parameters, etc.

3.1. Atom morphological evolution

Fig.1 shows the atom morphological evolution of $Ni_{75}Al_{10}Cr_{15}$ alloy during pre-ageing at 873 K. The lower pre-ageing temperature leads to a relatively higher saturation of alloy thus causing precipitated phases to emerge rapidly in the disordered matrix at 2 800 time step as shown in Fig.1(a). They are defined as DO_{22} phases by judging the color and 2D projection of the atoms. The atom appearances at 10 000 time step are shown in Fig.1(b), from which it is clear that some $L1_2$ phases begin to emerge and grow on the boundaries of DO_{22} phases. Al-rich zones, due to the diffusion of solute atoms, form on the boundaries of less-ordered DO_{22} phases, which gradually convert into $L1_2$ phases with the amount of DO_{22} phase beginning to decrease correspondingly. Simultaneously, some DO_{22} and $L1_2$ phases separately start to grow to the accompaniment of colliding, merging, and coarsening at the early stage of precipitation. It is corroborated by large quantities of DO_{22} and $L1_2$ phase nuclei existing in the matrix after pre-ageing at 873 K.

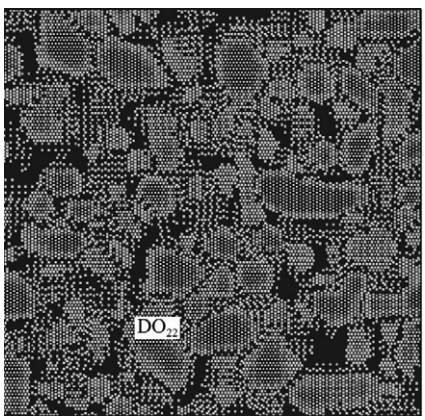

(a) 2 800 time steps

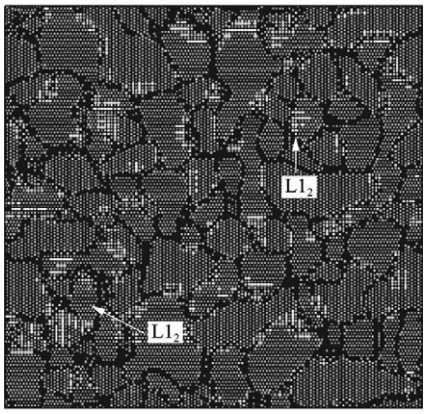

(b) 100 000 time steps

Fig.1 Atom morphology for $Ni_{75}Al_{10}Cr_{15}$ alloy during pre-ageing at 873 K.

After having pre-aged at 873 K, the $Ni_{75}Al_{10}Cr_{15}$ alloy is re-aged at 923 K, 1 023 K, and 1 123 K respectively. From the atom morphological evolution (see Fig.2), can be observed: ① The amount of precipitate phase decreases with the temperature rising and at 1 123 K, DO_{22} phases completely disappear with $L1_2$ phases alone present in the matrix. ② As the re-ageing goes on, particles of all sizes grow concurrently with colliding and merging; solute atoms in the smaller particles dissolve into the matrix and then diffuse into the larger particles; in this process, the smaller particles unceasingly shrink until completely disappearing while the larger particles continuously swell. In addition, as shown in Fig.2(c) and Fig.2(f), the particle-size of $L1_2$ phase increases while that of DO_{22} phase decreases as the re-ageing temperature rises from 923 K to 1 023 K. During re-ageing at 1 123 K, remarkable differences in size between individual $L1_2$ phase particles and significantly disordered regions can be observed in the matrix (see Fig.2(i)). ③At the late stage of coarsening process, elastic strain energy seems to exert much more effects on morphological evolution of precipitate phases at lower re-ageing temperature. Fig.2(c) shows the atom appearances at 1 000 000 time steps during re-ageing at 923 K. From it, it is clear that precipitate phase particles exhibit alignment along <100> direction to a certain extent. The effects of elastic strain on microstructure begin to weaken with the re-ageing temperature rising, and the precipitate phase particles become randomly distributed in the matrix at 1 123 K (see Fig.2(i)). As the temperature rises, the number of precipitate phase particles decreases and the elastic interaction arising from the overlap of the elastic strain fields weakens. In fact, in many Ni-based alloys there exists the same phenomenon caused by elastic strain energy as in Ni-Al-Ti aged microstructures discovered by T. Maebash, et al[15]. A. C. Lund, et al.[16] found the $L1_2$ phase particles that align themselves along <100> direction in Ni-Al system and Y. Nunomura, et al.[17] also discovered experimentally the same phenomenon in $L1_2$ and DO_{22} phases in the pseudo-ternary Ni_3Al-Ni_3Ti-Ni_3V system.

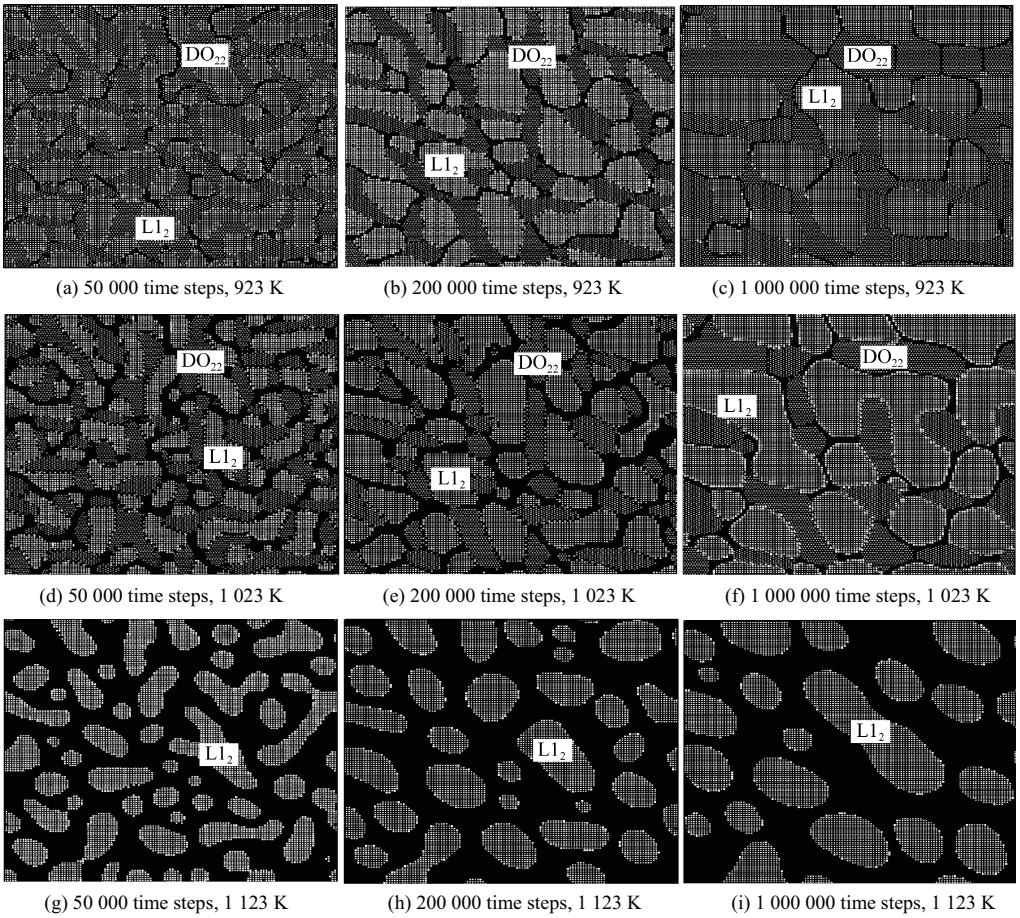

(a) 50 000 time steps, 923 K (b) 200 000 time steps, 923 K (c) 1 000 000 time steps, 923 K

(d) 50 000 time steps, 1 023 K (e) 200 000 time steps, 1 023 K (f) 1 000 000 time steps, 1 023 K

(g) 50 000 time steps, 1 123 K (h) 200 000 time steps, 1 123 K (i) 1 000 000 time steps, 1 123 K

Fig.2 Atomic morphology evolution for $Ni_{75}Al_{10}Cr_{15}$ alloy during re-ageing.

3.2. Nucleation mechanism

The difference between nucleation growth and spinodal decomposition is mainly attributed to the evolution of concentration within the ordered phase. Concentration at a site is defined by an average of occupation probabilities of the nearest-neighbor and the second-nearest neighbor sites, i.e.

$$C(i,j)=[P(i-1,j-1)+P(i-1,j)+P(i-1,j+1)+P(i,j-1)+P(i,j)+P(i,j+1)+P(i+1,j-1)+P(i+1,j)+P(i+1,j+1)]/9 \quad (7)$$

Ordering process can be described by a long order parameter expressed by[18]

$$\eta(i,j)=\frac{C(i,j)-P(i,j)}{C(i,j)\cos[\pi(i+j)]} \quad (8)$$

where $P(i, j)$ is the occupation probability of atoms, $C(i, j)$ the local concentration, $\eta(i, j)$ the long range order (LRO) parameter at the position (i, j).

Fig.3 shows the evolution of Cr-concentration and LRO parameter of Cr within DO_{22} phase of $Ni_{75}Al_{10}Cr_{15}$ alloy during pre-ageing at 873 K respectively. As shown in Fig.3(a), the concentration within DO_{22} phase slightly fluctuates at 1 800 time step and as the pre-ageing progresses, the concentration gradually rises with its range keeping constant. Meanwhile, the evolution of concentration is characterized by a concave in the middle with two prominent shoulders. This is because of the Cr solute atoms diffusing along phase boundaries that result in a temporary lack of Cr atoms at the center of DO_{22} phase. When the Cr solute atoms continue to diffuse, the middle part of the concentration curve becomes a plateau meaning the concentration finally reaches the equilibrium at 10 000 time step. The evolution of concentration within DO_{22} phase is in general agreement with the characteristics of spinodal decomposition that concentration slightly fluctuates in an extensive range. Fig.3(b) shows that the LRO parameter of DO_{22} phase rapidly reaches equilibrium at the time when the concentration of DO_{22} phase is far away from the equilibrium at 4 000 time step, which demonstrates that ordering process goes faster than atom clustering.

Fig.4 presents the evolution of Al-concentration and LRO parameter of Al within $L1_2$ phase of $Ni_{75}Al_{10}Cr_{15}$ alloy during pre-ageing at 873 K. From Fig.4(a), it is observed that the concentration evolution within $L1_2$ phase differentiates from that within DO_{22} phase in its slight fluctuation at 3 200 time step and its center much higher concentrated than the edge. As the pre-ageing

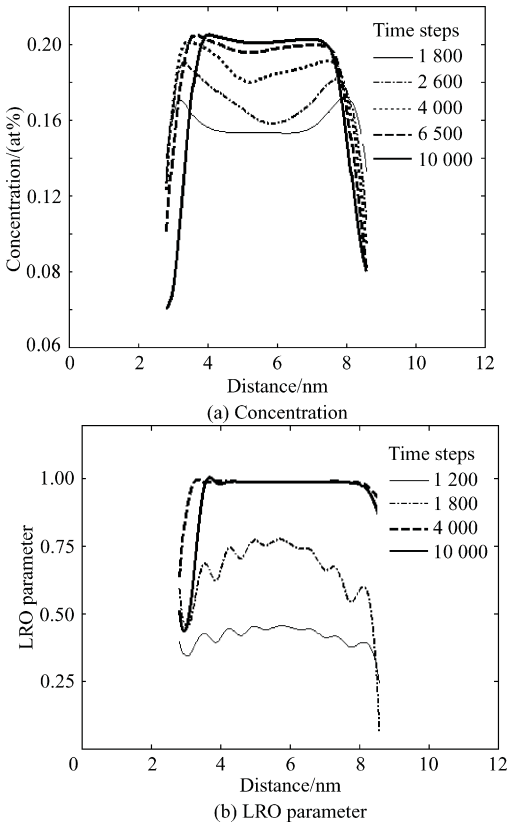

Fig.3 Evolution of Cr-concentration and LRO parameter of Cr within DO_{22} phase of $Ni_{75}Al_{10}Cr_{15}$ alloy during pre-ageing at 873 K.

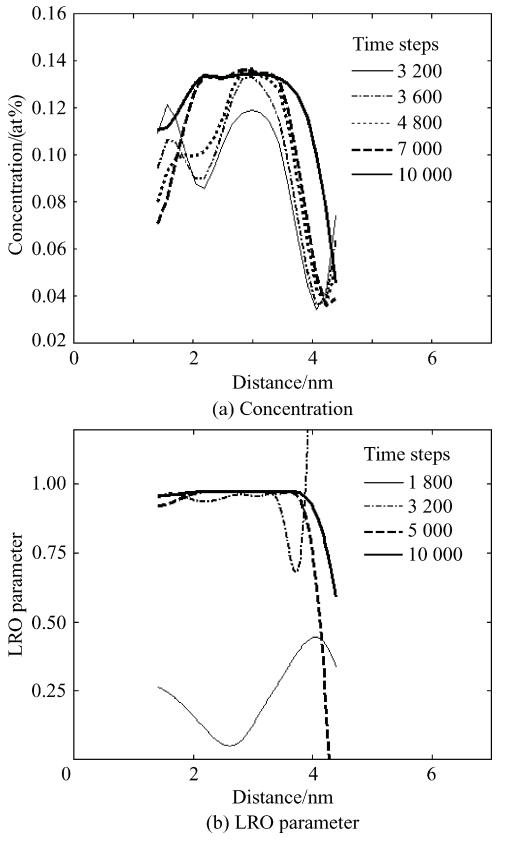

Fig.4 Evolution of Al-concentration and LRO parameter of Al within $L1_2$ phase of $Ni_{75}Al_{10}Cr_{15}$ alloy during pre-ageing at 873 K.

progresses, the middle part of the concentration curve of $L1_2$ phase slowly becomes a plateau meaning the concentration rises gradually to equilibrium. And then it continues to widen together with the growth of $L1_2$ phase. Moreover, the phase boundaries of $L1_2$ phase are characteristic of disperse interfaces. All these aforesaid corroborate that the $L1_2$ grows in accompany with non-classical nucleation. It can be seen from Fig.4(b) that the LRO parameter of $L1_2$ phase begins to slightly fluctuate at 1 800 time step and quickly rises to reach equilibrium at 3 200 time step. Similar to DO_{22} phase, in $L1_2$ phase, the ordering process is faster than atom clustering.

3.3. Particle density and radius

Fig.5 shows the particle density evolution within DO_{22} and $L1_2$ phases of $Ni_{75}Al_{10}Cr_{15}$ alloy during re-ageing at different temperatures. It can be observed that particle density within both DO_{22} and $L1_2$ phases soars to a peak and then drops at three different re-ageing temperatures, which means coarsening begins at the early stage. Their density decreases and reaches the maximum sooner at higher re-ageing temperature. The particle density of both $L1_2$ and DO_{22} phases decreases with the re-ageing temperature rising from 923 K to 1 123 K until equilibrium is reached.

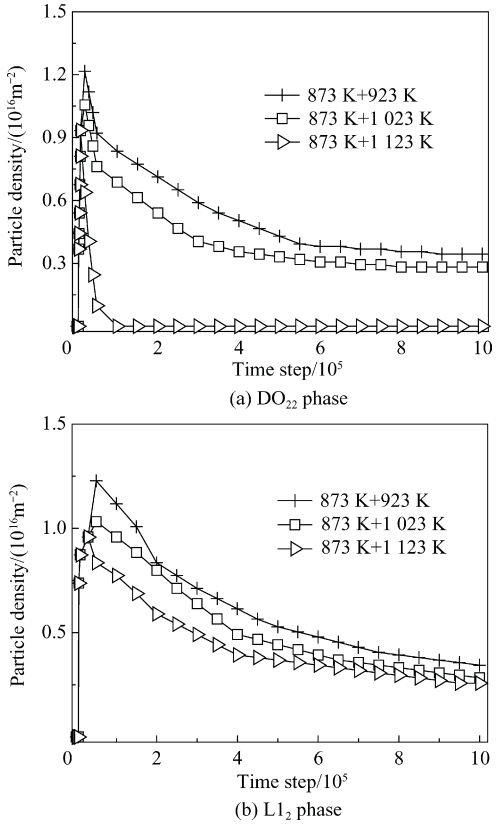

Fig.5 Particle density evolution of DO_{22} phase and $L1_2$ phase for $Ni_{75}Al_{10}Cr_{15}$ alloy during re-ageing at different temperatures.

Fig.6 shows the evolution of the cubes of averaged radius of DO_{22} phase and $L1_2$ phase in $Ni_{75}Al_{10}Cr_{15}$

alloy respectively during re-aging at different temperatures. With the re-ageing temperature rising from 923 K to 1 023 K, the averaged radius of either phase tends to increase though, the $L1_2$ phase grows much larger than the DO_{22} phase at the same time point. However, when the re-ageing temperature continues to increase to 1 123 K, the saturation degree of alloy decreases, both DO_{22} and $L1_2$ phases begin to dissolve with the averaged radius of $L1_2$ phase diminishing and that of DO_{22} phase gradually disappearing.

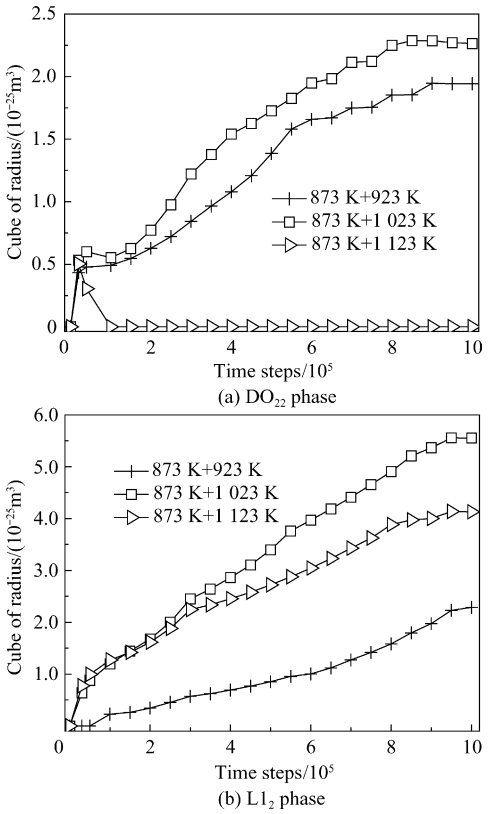

Fig.6 Evolution of cube of averaged radius of DO_{22} phase and $L1_2$ phase for $Ni_{75}Al_{10}Cr_{15}$ alloy during re-aging at different temperatures.

In conclusion, when submitting $Ni_{75}Al_{10}Cr_{15}$ alloy to re-ageing at different temperatures, the particle density decreases but the averaged radius increases. The time-dependent increase of cube of averaged radius of DO_{22} and $L1_2$ phases is characterized by absence of a linear relationship, which, if any, exists only in the early stage of coarsening. The so-called LSW theory and its extension under the condition of limited volume fraction describes the dynamics of the Ostwald ripening, in which one of the phases fills a very small volume fraction of the system and the driving force of coarsening is assumed to be only the surface energy. When taking into account the effects of strain on the coarsening of particles, on the whole, the coarsening behavior of two phases fails to follow the time-law predictions by LSW diffusion-controlled growth theory.

3.4. Evolution of volume fraction

Fig.7 shows the volume fraction evolution of DO_{22} and $L1_2$ phases in $Ni_{75}Al_{10}Cr_{15}$ alloy during two-step ageing. It can be observed that there are two features: ① With the re-ageing temperature rising, the volume fraction of DO_{22} phase decreases to zero while the volume fraction of $L1_2$ phase first increases and then decreases, which can be explained by both DO_{22} and $L1_2$ phases starting to dissolve at very high re-ageing temperatures. ② As re-ageing progresses, the volume fraction of DO_{22} phase first attains a peak and then begins to decrease with slight increase following again, but the $L1_2$ phase changes in a relatively gentle manner. It can be ascribed to there being full of competing and compromising between DO_{22} phase and $L1_2$ phase in all stages of the whole precipitation process, and the way the alloy behaves depends on which phase would be at an advantage in each stage.

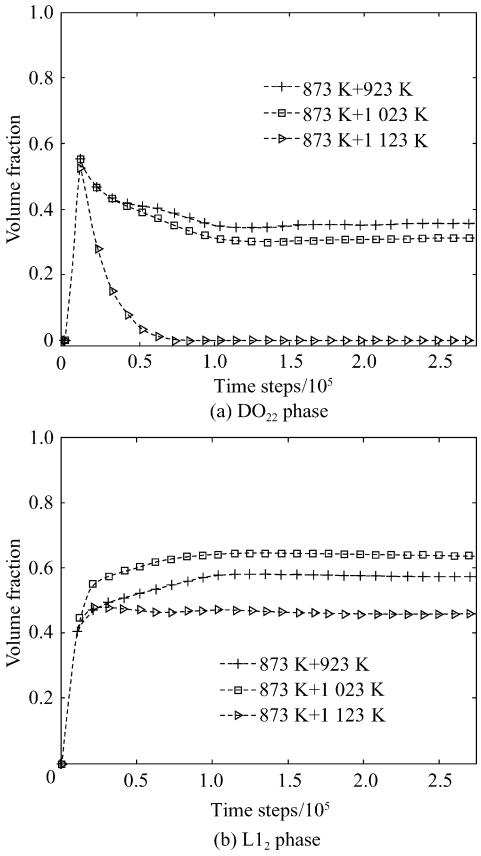

Fig.7 Evolution of DO_{22} phase volume fraction and $L1_2$ phase volume fraction for $Ni_{75}Al_{10}Cr_{15}$ alloy during ageing and re-ageing.

4. Conclusions

(1) In the pre-ageing stage, DO_{22} phase first form through spinodal decomposition mechanism, and then $L1_2$ phase begins to emerge on the DO_{22} phase boundaries through a non-classical nucleation mechanism. The ordering process of both DO_{22} and $L1_2$ phases goes faster than atom clustering.

(2) Elastic strain energy exerts much more effects on the morphology of precipitate phases, and DO_{22} and $L1_2$ phases exhibit directional alignment along ⟨100⟩

direction to a certain extent at lower re-ageing temperatures. With the re-ageing temperature increasing, the precipitate phase begins to dissolve thus soothing the influences from the elastic strain energy and having ordered phases randomly distributed in the matrix. Taking account of the effects of elastic strain energy, on the whole, the coarsening behavior of two phases fails to follow the time-law predictions by LSW diffusion-controlled growth theory.

(3) The volume fraction of DO_{22} phase decreases to zero, whereas that of $L1_2$ phase first increases and then decreases with the temperature rising from 923 K to 1 123 K, which indicates existence of competing and compromising between DO_{22} phase and $L1_2$ phase in every stage of the whole precipitation process.

References

[1] Sudbrack C K, Yoon K E, Noebe R D, et al. Temporal evolution of the nanostructure and phase compositions in a model Ni-Al-Cr alloy. Acta Materialia 2006; 54(12): 3199-3210.

[2] Sudbrack C K, Noebe R D, Seidman D N. Compositional pathways and capillary effects during isothermal precipitation in a nondilute Ni-Al-Cr alloy. Acta Materialia 2007; 55(1): 119-130.

[3] Fischer R, Eleno L T F, Frommeyer G, et al. Precipitation of Cr-rich phases in a Ni-50Al-2Cr (at.%) alloy. Intermetallics 2006; 14(2): 156-162.

[4] Hou G C, Wei H, Zhao N R, et al. Interdiffusion in the β phase region of the Ni-Al-Cr system. Scripta Materialia 2008; 58(1): 57-60.

[5] Brož P, Svoboda M, Buršík J, et al. Theoretical and experimental study of the influence of Cr on the γ+γ′ phase field boundary in the Ni-Al-Cr system. Materials Science and Engineering A 2002; 325(1-2): 59-65.

[6] Poduri R, Chen L Q. Computer simulation of the kinetics of order-disorder and phase separation during precipitation of δ′ (Al_3Li) in Al-Li alloys. Acta Materialia 1997; 45(1): 245-255.

[7] Lu Y L, Chen Z, Wang Y X. Microscopic phase-field simulation of the early precipitation mechanism of Ni_3Al phase in Ni-Al alloys. Materials Letters 2008; 62(8-9): 1385-1388.

[8] Poduri R, Chen L Q. Computer simulation of atomic ordering and compositional clustering in the pseudobinary Ni_3Al-Ni_3V system. Acta Materialia 1998; 46(5): 1719-1729.

[9] Li Y S, Chen Z, Lu Y L, et al. Computer simulation for the precipitation process of $Ni_{75}Al_{7.5}V_{17.5}$ alloy. Progress in Natural Science 2004; 14 (12): 1099-1103.

[10] Khachaturyan A G. Theory of structural transformation in solids. New York: Wiley, 1983.

[11] Onuki A. Ginzburg-Landau approach to elastic effects in the phase separation of solids. Journal of the Physical of Japan 1989; 58: 3065-3068.

[12] Pareige C, Soisson F, Martin G, et al. Ordering and phase separation in Ni-Cr-Al: Monte Carlo simulations VS three-dimensional atom probe. Acta Materialia 1999; 47(6): 1889-1899.

[13] Prikhodko S V, Carnes J D, Isaak D G, et al. Elastic constants of a Ni-12.69%Al alloy from 295 to 1 300 K. Scripta Materialia 1998, 38(1): 67-72.

[14] Duval S, Chambreland S, Caron P, et al. Phase composition and chemical order in the single crystal nickel base superalloy MC2. Acta Metallurgica et Materialia 1994; 42(1): 185-194.

[15] Maebashi T, Doi M. Coarsening behaviours of coherent γ′ and γ precipitates in elastically constrained Ni-Al-Ti alloys. Materials Science and Engineering A 2004; 373 (1-2): 72-79.

[16] Lund A C, Voorhees P W. The effects of elastic stress on coarsening in the Ni-Al system. Acta Materialia 2002; 50(8): 2085-2098.

[17] Nunomura Y, Kaneno Y, Tsuda H, et al. Phase relation and microstructure in multi-phase intermetallic alloys based on Ni_3Al-Ni_3Ti-Ni_3V pseudo-ternary alloy system. Intermetallics 2004; 12(4): 389-399.

[18] Chen L Q, Simmons J A. Microscopic master equation approach to diffusional transformations in inhomogeneous systems-single-site approximation and direct exchange mechanism. Acta Metallurgica et Materialia 1994; 42(9): 2943-2954.

Biographies:

Zhang Jixiang Born in 1974, he received B.S. and M.S. degrees from Chongqing University in 1998 and Xi'an University of Architecture and Technology in 2005 respectively. Now he works as a Ph.D. candidate in Northwestern Polytechnical University. His main research interest lies in computational material science.
E-mail: zhangjixiangdoctor@yahoo.com.cn

Chen Zheng Born in 1952, he is a professor and Ph.D. supervisor in Northwestern Polytechnical University. His main research interests include materials computation design and rare earth materials.
E-mail: chenzh@nwpu.edu.cn